GPS Solut
DOI 10.1007/s10291-011-0240-x

ORIGINAL ARTICLE

# Integrated GPS/INS navigation system with dual-rate Kalman Filter

**Songlai Han · Jinling Wang**

Received: 1 January 2011 / Accepted: 3 September 2011


**Abstract** A dual-rate Kalman Filter (DRKF) has been developed to integrate the time-differenced GPS carrier phases and the GPS pseudoranges with INS measurements. The time-differenced GPS carrier phases, which have low noise and millimeter measurement precision, are integrated with INS measurements using a Kalman Filter with high update rates to improve the performance of the integrated system. Since the time-differenced GPS carrier phases are only relative measurements, when integrated with INS, the position error of the integrated system will accumulate over time. Therefore, the GPS pseudoranges are also incorporated into the integrated system using a Kalman Filter with a low update rate to control the accumulation of system errors. Experimental tests have shown that this design, compared to a conventional design using a single Kalman Filter, reduces the coasting error by two-thirds for a medium coasting time of 30 s, and the position, velocity, and attitude errors by at least one-half for a 45-min field navigation experiment.

**Keywords** GPS · INS · Sensor integration · Dual-rate Kalman Filter

S. Han (✉)
College of Opto-Electric Science and Engineering,
National University of Defense Technology,
Changsha, Hunan, People's Republic of China
e-mail: hansonglai@hotmail.com

J. Wang
School of Surveying and Spatial Information Systems,
The University of New South Wales, Sydney,
NSW 2052, Australia
e-mail: Jinling.Wang@unsw.edu.au

## Introduction

Although the integration of GPS and INS has been investigated intensively (Groves 2008; Grewal et al. 2007), but a reflection of the motivations for such integration is beneficial. GPS has long-term stability, and there is no error accumulation over time. However, GPS depends on the environment, i.e., GPS signals can be easily affected by city canyons, high buildings, or trees. The INS is completely autonomous, and generally has a high update rate with the attitude output. However, INS errors are time dependent, which means the performance will degrade with time, because of the error accumulation of the inertial sensors. Integration of GPS and INS can incorporate their benefits of both and overcome their individual drawbacks. Specifically, the motivations of integration can be summarized as: (a) providing long-term high-accuracy navigation solutions when the GPS signals are intact and (b) providing coasting ability to bridge the GPS outages when the GPS signals are blocked. We focus on maximizing the gains for these two motivations.

However, both of the commonly utilized GPS observations, pseudoranges and carrier phases, cannot well fulfill the requirements of the integrated system for land vehicle applications. Now, the pseudoranges have an accuracy of several meters up to several tens of meters during normal operations (IS-GPS-200D 2006; GPS SPS PS 2008). Therefore, when the GPS pseudoranges are integrated with INS, both the navigation accuracy and the coasting performance of the integrated system are poor. The non-compensable errors, namely the receiver noise and multipath (RNM), of the GPS carrier phases are 100 times less than those of the pseudoranges (Misra and Enge 2001). However, the real-time integer ambiguity resolution is still a challenging issue for navigation applications (Zheng and

Published online: 02 October 2011

Gebre-Egziabher 2009; Banville and Langley 2009; Wang et al. 1998, 2000).

The time-differenced GPS carrier phase (Farrell 2001, 2006; Graas and Soloviev 2004) is a precise and unambiguous measurement. It is anticipated that, if integrated with INS, the time-differenced carrier phases can dramatically improve the navigation performances of the integrated system. However, the experimental tests discussed below have shown that the integration of the time-differenced carrier phases and INS can achieve very good performance over short term, but it will introduce position error accumulation in the long run. This arises from the fact that the time-differenced carrier phases are only relative measurements in nature, so when they are integrated with INS, the absolute position error of the integrated system cannot be corrected.

We have designed a dual-rate Kalman Filter to fix the above problem. A high-rate Kalman Filter, with the same update rate as the GPS receiver, generally 1 Hz, has been developed to integrate the time-differenced carrier phases and INS measurements. This high-rate Kalman Filter is mainly used to provide a high-accuracy relative aiding and to improve the short-term navigation precision and the coasting ability of the integrated system. A low-rate Kalman Filter, with the frequency of 0.01 Hz, has also been developed to integrate the pseudoranges and INS measurements. This low-rate Kalman Filter is mainly used to limit the position error of the integrated system and to keep the long-term navigation accuracy. The high-rate and low-rate Kalman Filters are coupled together through the system error dynamics of GPS/INS integration to form the dual-rate Kalman Filter. Our experimental tests have shown that this design based on the dual-rate Kalman Filter has dramatically improved the navigation accuracy and the coasting performance of the GPS/INS integrated navigation system with less computation burden.

## Review of GPS/INS integration for navigation applications

In navigation applications, it is required that the navigation information should be provided continuously in real time. So a conventional choice for GPS/INS integrated navigation system is based on the fusion of stand-alone GPS pseudoranges and INS measurements.

The integration of GPS pseudorange and INS can be implemented by, e.g., loosely coupled integration and tightly coupled integration approaches. The loosely coupled integration can only operate when the number of the observed satellites in the sky is more than four, while the tightly coupled integration can still operate when the number of the observed satellites is less than four (Groves 2008). Considering this superiority, only the tightly coupled integration is discussed herein.

The schematic diagram of the tightly coupled integration of GPS pseudoranges and INS measurements is shown in Fig. 1. The GPS navigation messages are used to compute the observed satellites positions, and then, the GPS receiver position computed from INS together with the satellites positions is utilized to predict the pseudoranges between the GPS receiver and the satellites. Then, the pseudorange errors between the predicted pseudoranges and the observed pseudoranges from the GPS receiver are input into the Extended Kalman Filter to optimally estimate the system errors including the position, velocity and attitude (PVA) errors, and the inertial sensor drifts. Finally, the PVA errors are utilized to correct the PVA computed from INS, and meanwhile, the estimated inertial sensor drifts are utilized to calibrate the inertial sensors. The test results regarding this conventional approach of GPS/INS integrated navigation system is presented in "Experimental tests and analysis".

From Fig. 1, it can be noticed that the observed pseudoranges from the GPS receiver are utilized as a reference, and their differences with the predicted pseudoranges are input into the Extended Kalman Filter to estimate the navigation errors and the drifts of the inertial sensors. Because the error of the observed pseudoranges from the GPS receiver is at the level of several meters, the navigation errors and the drifts of the inertial sensors output from the Extended Kalman Filter can only be as good as such level. This will lead to low navigation accuracy and poor coasting performance.

A possible way to reduce the errors of the pseudoranges is using carrier phases to smooth them. Carrier phase smoothed–pseudoranges have both the merits of the pseudorange and the carrier phase. However, the carrier phase–smoothed pseudoranges are generally computed from a recursive filter of certain length, which might last for tens of seconds to tens of minutes. This means that a restart time depending on the filter length is necessary if cycle slips or signal dropout occurs. This restart time will affect the continuity of navigation, especially in city canyons or similar circumstances.

## Time-differenced carrier phases and their applications in GPS/INS integration

The measurement equation of GPS carrier phase can be expressed as (Misra and Enge 2001),

$$\varphi = \lambda^{-1}(r - I + T) + \lambda^{-1}c(\delta t_u - \delta t^s) + N + \varepsilon \qquad (1)$$

where $\lambda$ and $c$ are the wavelength and wave velocity of the carrier; $r$ is the geometric distance between the satellite and

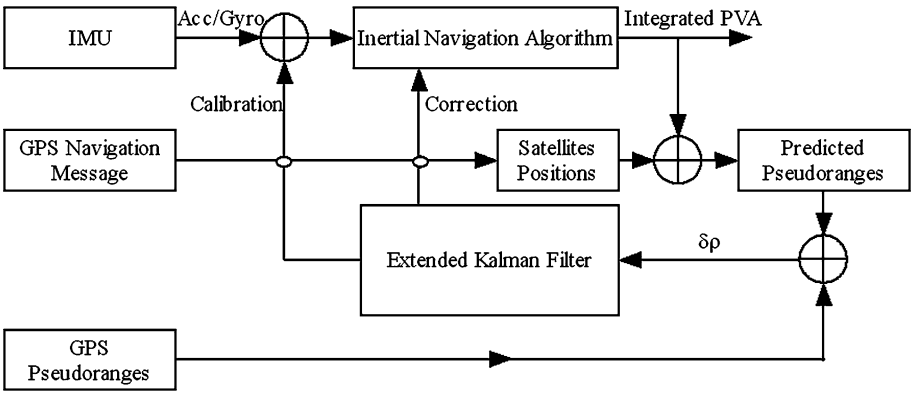


**Fig. 1** Tightly coupled integration of GPS pseudoranges and INS measurements

user receiver; $I$ and $T$ are the ionospheric and tropospheric delay of the carrier in the atmosphere; $\delta t_u$ and $\delta t^s$ are the errors of the user clock and the satellite clock; $N$ is the integer ambiguity, and $\varepsilon$ represents the noise in the carrier phase.

In order to use the carrier phase in real-time navigation applications, the unknown integer $N$ should be removed first, which can be achieved by time-differencing the carrier phase observable (Farrell 2001, 2006; Graas and Soloviev 2004),

$$\varphi_{\Delta t} = -\lambda^{-1} \cdot \overrightarrow{e(t_2)} \cdot \overrightarrow{\Delta b} + \lambda^{-1} c \cdot \Delta\delta t_u + \Delta\varepsilon \tag{2}$$

where $\varphi_{\Delta t}$ is the time-differenced carrier phase, which has been compensated for the ionospheric and tropospheric delays and adjusted for the satellite Doppler and geometry changes. Let $t_1$ and $t_2$ represent the previous epoch and current epoch, and then, $\overrightarrow{e(t_1)}$ and $\overrightarrow{e(t_2)}$ represents the unit vectors of the line-of-sight direction from the GPS receiver to the satellites at $t_1$ and $t_2$, respectively. The quantity $\overrightarrow{\Delta b}$ is the vector of the position increment of the user receiver from $t_1$ to $t_2$. The quantity $\Delta\delta t_u$ represents the clock error drift of the user receiver. As is known, the clock error $\delta t_u$ in (1) can be removed by differencing measurements of two concurrently observed satellites. The clock error drift $\Delta\delta t_u$ in (2) can also be removed by using the same method. A more concise form of the time-differenced carrier phase measurement can be obtained as,

$$\varphi_{\Delta t}^{ij} = \lambda^{-1} \cdot \left(\overrightarrow{e_j(t_2)} - \overrightarrow{e_i(t_2)}\right) \cdot \overrightarrow{\Delta b} + \Delta\varepsilon_{ij} \tag{3}$$

where $i$ and $j$ represent two concurrently observed satellites, and $\varphi_{\Delta t}^{ij}$ represents the difference of $\varphi_{\Delta t}$ between satellites $i$ and $j$. The quantities $\overrightarrow{e_i(t_2)}$ and $\overrightarrow{e_j(t_2)}$ are the unit vectors of the line-of-sight from the user receiver to satellites $i$ and $j$, respectively.

From (2) and (3), it can be observed that the time-differenced carrier phases $\varphi_{\Delta t}$ or $\varphi_{\Delta t}^{ij}$ have two characteristics: high-precision and no integer ambiguity. If they are integrated with INS, the navigation accuracy and coasting performance of the integrated system should be improved. As discussed above, $\overrightarrow{\Delta b}$ in (2) and (3) is the position increment of the user receiver in two consecutive GPS epochs $t_1$ and $t_2$. So the average velocity of the user receiver between $t_1$ and $t_2$ can be easily derived from $\overrightarrow{\Delta b}$. Especially, if the GPS update rate is 1 Hz, namely the time difference between $t_1$ and $t_2$ being 1 s, $\overrightarrow{\Delta b}$ itself will be the average velocity. It can be observed that $\overrightarrow{\Delta b}$ can be easily computed from (2) or (3) by using the least squares method, if the number of the observed satellites is more than four. Van Graas and Soloviev (2004) provided a detailed procedure to compute the average velocity by using (2). Han and Wang (2010) computed the average velocity from (3), and then, the obtained velocity together with the position computed from the pseudoranges was integrated with INS to provide a robust solution for land vehicle navigation. Similar to other loosely coupled integrations, the integration of the velocity computed from the time-differenced carrier phase and INS can only operate under the condition that there are at least four observed satellites in the sky.

Apart from the velocity computed from (2) or (3), the original time-differenced carrier phase in (2) or (3) can also be directly used in GPS/INS integrated navigation. Wendel and Trommer (2004) and Wendel et al. (2006) discussed the tightly coupled integration of the time-differenced carrier phase and INS. However, the derivation of the measurement model in Wendel and Trommer (2004) and Wendel et al. (2006), which is the essential part of the integration, was wrong.

We have implemented the tightly coupled integration of the time-differenced carrier phases and INS measurements, and the navigation errors are shown in Fig. 2. It can be found that the position errors in Fig. 2 were slowly accumulated with time. Through theoretical and experimental analysis, it was found that the accumulation of the position error was introduced by the fact that the time-differenced carrier phase is only a relative measurement between consecutive epochs, and there is no absolute position

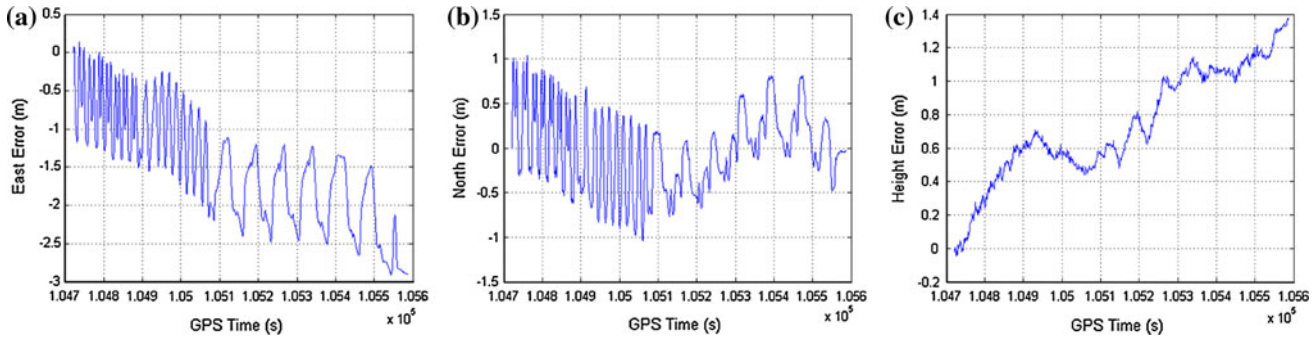


**Fig. 2** The position errors from the integration of time-differenced carrier phase and INS. The panels show: **a** east error, **b** north error, and **c** height error

information included in it. In order to introduce the absolute position information into the integrated system, the pseudoranges, together with the time-differenced carrier phases, will be introduced into the integrated navigation system in a novel and effective way in this research, which will be discussed in the next section.

## A dual-rate Kalman Filter design for GPS/INS integration

The schematic diagram of the proposed dual-rate Kalman Filter is shown in Fig. 3. Assume the GPS receiver has an update rate of 1 Hz and the INS has an update rate of 100 Hz. The position accumulator in Fig. 3 will accumulate the INS position change in 1 s by adding the 100 times position increments. Following this, the obtained INS position change will be first compensated by the change of the lever arm between the INS center and the GPS antenna, and then be used to estimate the position change of the GPS antenna, $\widehat{\overrightarrow{\Delta b}}$. According to (3), the estimated change of the GPS antenna, $\widehat{\overrightarrow{\Delta b}}$, is then projected on the line-of-sight (LOS) of the observed satellites to estimate the time-differenced carrier phase. Finally, the difference between the estimated time-differenced carrier phase and the observed time-differenced carrier phase is computed and input into the Extended Kalman Filter H to estimate the PVA errors and the drifts of the inertial sensors, which are then feedback to the INS to correct the PVA errors and to calibrate the inertial sensors. The Extended Kalman Filter H is the high-rate Kalman Filter and will be carried out with the same update rate as the GPS receiver, namely 1 Hz in the above case.

The Extended Kalman Filter L in Fig. 3 is the low-rate Kalman Filter, which is quite similar with the one used in the conventional integration in Fig. 1, except the following two differences. One is that the outputs of the Extended Kalman Filter L will not compensate the drifts of the inertial sensors and the other one is that the Extended Kalman Filter L is carried out with a low update rate, 0.01 Hz, namely one hundredth of the update rate of the Extended Kalman Filter H. Both of the differences arise from the fact that the accuracy of the GPS pseudorange is low, which will lead to low accuracy of the estimated drifts of the inertial sensors and the estimated errors of the PVA. Therefore, the outputs of the Extended Kalman Filter L are utilized to correct the PVA in a very low rate to reduce the noises in the integrated PVA.

The proposed dual-rate Kalman Filter design for GPS/INS integration can dramatically reduce the computation burden. If the time-differenced carrier phase and the pseudoranges were processed in a single Kalman Filter, the dimensions of the measurement matrix will be very large, which will increase the computation burden. In the proposed dual-rate Kalman Filter design, the two types of measurements are processed separately, so a large measurement matrix is divided into two smaller ones, and the computation burden is reduced.

The Extended Kalman Filter H and L are the essential parts of this design. To implement a Kalman Filter, the process model and the measurement model should be determined first as,

$$\dot{X} = FX + u \tag{4}$$

$$Z = HX + v \tag{5}$$

Equation 4 is the process model, and Equation 5 is the measurement model. The Kalman Filter H and L share the same process model, which is based on the system error dynamics. The system error dynamics is derived from the INS error equations by expanding some of the error terms. The measurement models are different for the Kalman Filter H and L. For Kalman Filter H, the measurement model should be derived from the observation equation of the time-differenced carrier phase, namely Eq. 3. For Kalman Filter L, the measurement model should be derived from the observation equation of pseudorange (Misra and Enge 2001). The derivations for the process model and the

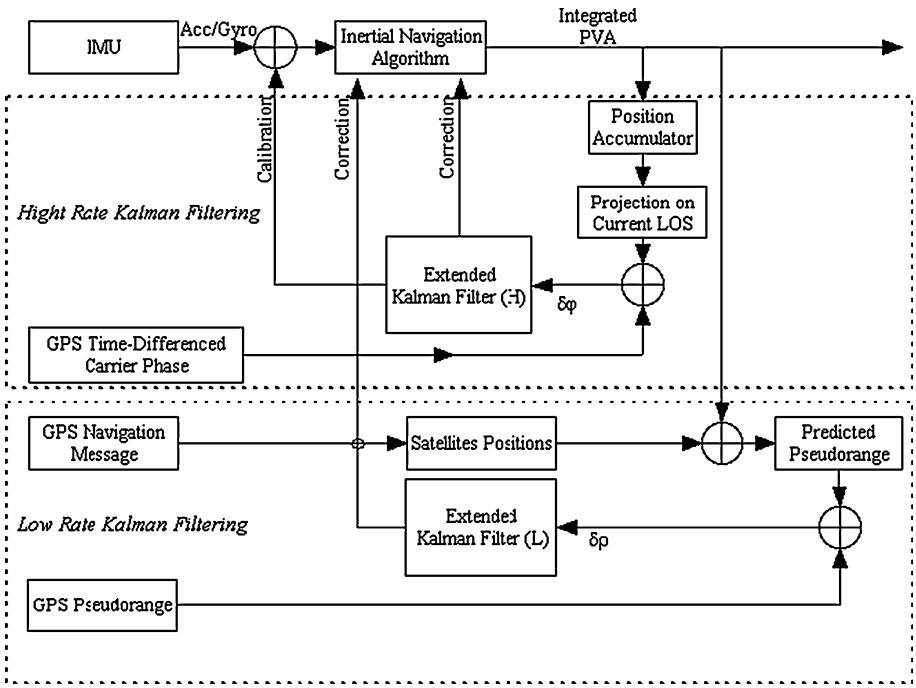


**Fig. 3** GPS/INS integration based on proposed dual-rate Kalman Filtering

measurement models of the Kalman Filter H and L will proceed as follows.

System error dynamics of GPS/INS integration

The system error dynamics of GPS/INS integration is based on the INS error equations. The psi-angle error equations of INS are as follows (Goshen-Meskin and Bar-Itzhack 1992),

$$\delta\dot{\vec{r}} = \delta\vec{v} - \vec{\omega}_{ec} \times \delta\vec{r} \tag{6}$$

$$\delta\dot{\vec{v}} = -(\vec{\omega}_{ic} + \vec{\omega}_{ie}) \times \delta\vec{v} - \vec{\psi} \times \vec{f} + \delta\vec{g} + \vec{\nabla}' \tag{7}$$

$$\dot{\vec{\psi}} = -\vec{\omega}_{ic} \times \vec{\psi} + \vec{\varepsilon}' \tag{8}$$

The system error dynamics of GPS/INS integration is obtained by expanding the gravity anomaly vector, $\delta\vec{g}$, the accelerometer error vector, $\vec{\nabla}'$, and the gyro error vector, $\vec{\varepsilon}'$.

According to Jekeli (1997) and Gebre-Egziabher and Wang (1998), the gravity anomaly can be viewed as a stochastic process and can be modeled using Gauss–Markov process. In this implementation, the gravity anomaly is modeled as a first-order Gauss–Markov process,

$$\delta\dot{\vec{g}} = -A_g\delta\vec{g} + G_g\vec{u}_g \tag{9}$$

where $\vec{u}_g$ is a unit white Gauss noise vector, and $A_g$ and $G_g$ are the coefficients matrix containing the time constant and the variance of Gauss–Markov process. The quantities $A_g$ and $G_g$ can be expressed as,

$$A_g = \begin{bmatrix} \beta & 0 & 0 \\ 0 & \beta & 0 \\ 0 & 0 & \beta \end{bmatrix} \tag{10}$$

$$G_g = \begin{bmatrix} \sqrt{2\sigma^2\beta} & 0 & 0 \\ 0 & \sqrt{2\sigma^2\beta} & 0 \\ 0 & 0 & \sqrt{2\sigma^2\beta} \end{bmatrix} \tag{11}$$

where $1/\beta$ is the time constant and $\sigma^2$ is the variance of Gauss–Markov process.

According to Wang et al. (2003), Niu and El-Sheimy (2005), and Han and Wang (2008), both the accelerometer error and the gyro error are modeled as the hybrid of a random walk process and a white Gaussian noise,

$$\vec{\nabla}' = \vec{\nabla} + \vec{u}_{\nabla'} \tag{12}$$

$$\vec{\varepsilon}' = \vec{\varepsilon} + \vec{u}_{\varepsilon'} \tag{13}$$

The white Gaussian noise vectors, $\vec{u}_{\nabla'}$ and $\vec{u}_{\varepsilon'}$, are directly used as the driving noise of the INS error equations, and the random walk process vectors, $\vec{\nabla}$ and $\vec{\varepsilon}$, are modeled as follows,

$$\dot{\vec{\nabla}} = \vec{u}_{\nabla} \tag{14}$$

$$\dot{\vec{\varepsilon}} = \vec{u}_{\varepsilon} \tag{15}$$

where $\vec{u}_{\nabla}$ and $\vec{u}_{\varepsilon}$ are also white Gaussian noise vectors.

For GPS/INS integration, the lever arm error should be also modeled. The lever arm is the vector from the center of INS to the center of the GPS antenna. This vector is measurable before the start-up of the system. However, the lever arm may suffer from flexure or distortion during operation, so its error should be compensated on the fly. In this implementation, the lever arm error is modeled as a random constant vector,

$$\delta\dot{\vec{l}} = 0 \tag{16}$$

More complicated stochastic models, such as Gauss–Markov processes, can also be used to model the lever arm error based on the characteristics of the lever arm changes. However, a random constant model is generally enough for most of short lever arm applications, such as land vehicle navigation.

Combining Eqs. 6–9 and 12–16, the system error dynamics of GPS/INS integration can be expressed as,

$$\begin{cases} \dot{\delta\vec{r}} = \delta\vec{v} - \vec{\omega}_{ec} \times \delta\vec{r} \\ \dot{\delta\vec{v}} = -(\vec{\omega}_{ic} + \vec{\omega}_{ie}) \times \delta\vec{v} - \vec{\psi} \times \vec{f} + \delta\vec{g} + \vec{\nabla} + \vec{u}_{\nabla'} \\ \dot{\vec{\psi}} = -\vec{\omega}_{ic} \times \vec{\psi} + \vec{\varepsilon} + \vec{u}_{\varepsilon'} \\ \dot{\delta\vec{g}} = -A_g \delta\vec{g} + G_g \vec{u}_g \\ \dot{\vec{\nabla}} = \vec{u}_{\nabla} \\ \dot{\vec{\varepsilon}} = \vec{u}_{\varepsilon} \\ \dot{\delta\vec{l}} = 0 \end{cases} \tag{17}$$

The above system error dynamics of GPS/INS integration can be rewritten in the matrix form,

$$\dot{x} = Fx + u \tag{18}$$

where $x$ is the error state vector, $F$ is the system matrix, and $u$ is the process noise vector. The expressions of $x$, $F$, and $u$ are,

$$x = \begin{bmatrix} \delta\vec{r} \\ \delta\vec{v} \\ \vec{\psi} \\ \delta\vec{g} \\ \vec{\nabla} \\ \vec{\varepsilon} \\ \delta\vec{l} \end{bmatrix},$$

$$F = \begin{bmatrix} -\vec{\omega}_{ec}\times & I & 0 & 0 & 0 & 0 & 0 \\ 0 & -(\vec{\omega}_{ic} + \vec{\omega}_{ie})\times & \vec{f}\times & I & I & 0 & 0 \\ 0 & 0 & -\vec{\omega}_{ic}\times & 0 & 0 & I & 0 \\ 0 & 0 & 0 & -A_g & 0 & 0 & 0 \\ 0 & 0 & 0 & 0 & 0 & 0 & 0 \\ 0 & 0 & 0 & 0 & 0 & 0 & 0 \\ 0 & 0 & 0 & 0 & 0 & 0 & 0 \end{bmatrix},$$

$$u = \begin{bmatrix} 0 \\ \vec{u}_{\nabla'} \\ \vec{u}_{\varepsilon'} \\ G_g u_g \\ \vec{u}_{\nabla} \\ \vec{u}_{\varepsilon} \\ 0 \end{bmatrix} \tag{19}$$

where $I$ is the three-dimensional identity matrix, and $\overrightarrow{(\cdot)}\times$ represents the skew symmetric matrix of vector $\overrightarrow{(\cdot)}$ (Savage 1998).

## Measurement model based on time-differenced carrier phases

The measurement model of the Extended Kalman Filter H in Fig. 3 can be derived from the observation equation of the time-differenced carrier phases, namely Eq. 3. For convenience, define a new variable $Y_i$ to represent the time-differenced carrier phases, and (3) can be rewritten as,

$$Y_i = \varphi_{\Delta t}^{ij} = -\lambda^{-1} \cdot \left(\overrightarrow{e_j(t_2)} - \overrightarrow{e_i(t_2)}\right) \cdot \overrightarrow{\Delta b} + \Delta\varepsilon_{ij} \tag{20}$$

The above equation is in vector form. By projecting the vectors into the navigation frame, the matrix form of the above equation can be written as follows,

$$Y_i = -\lambda^{-1} \cdot \left[C_e^n(t_2) \cdot \left(\overrightarrow{e_j(t_2)^e} - \overrightarrow{e_i(t_2)^e}\right)\right]^T \cdot \overrightarrow{\Delta b^n} + \Delta\varepsilon_{ij} \tag{21}$$

where $C_e^n(t_2)$ is the direction cosine matrix from the earth-centered earth-fixed frame (e frame) to the navigation frame (n frame), and the superscripts of the vectors represent the frames in which the vectors are projected. The quantity $\overrightarrow{\Delta b^n}$ in (21) represents the position increment of the GPS antenna from $t_1$ to $t_2$, and its relationship with the position increment of the INS center is as follows,

$$\overrightarrow{\Delta b^n} = \overrightarrow{\Delta b_{INS}^n} + \overrightarrow{l(t_2)^n} - \overrightarrow{l(t_1)^n} \tag{22}$$

where $\overrightarrow{\Delta b_{INS}^n}$ is the position increment of the INS center, and $\overrightarrow{l(t_2)^n}$ and $\overrightarrow{l(t_1)^n}$ represent the lever arm at $t_2$ and $t_1$, respectively. Considering the $\overrightarrow{\Delta b_{INS}^n}$ can be obtained by integrating the INS velocity, Eq. 22 can be transformed as,

$$\overrightarrow{\Delta b^n} = \int_{t_1}^{t_2} \overrightarrow{v_{INS}^n} \mathrm{d}t + C_b^n(t_2)\overrightarrow{l^b} - C_b^n(t_1)\overrightarrow{l^b} \tag{23}$$

where $\overrightarrow{v_{INS}^n}$ is the INS velocity projected into the navigation frame, $C_b^n(t_2)$ and $C_b^n(t_1)$ represent the direction cosine matrix from the body frame (b frame) to the navigation frame (n frame) at $t_2$ and $t_1$, respectively, and $\overrightarrow{l^b}$ represent the measured lever arm in the body frame. Insert (23) into (21), and the observation equation of the time-differenced carrier phase in the matrix form can be obtained as,

$$Y_i = -\lambda^{-1} \cdot \left[ C_e^n(t_2) \cdot \left( \overrightarrow{e_j(t_2)^e} - \overrightarrow{e_i(t_2)^e} \right) \right]^T \cdot \left( \int_{t_1}^{t_2} \overrightarrow{v_{\mathrm{INS}}^n} \mathrm{d}t + C_b^n(t_2) \overrightarrow{l^b} - C_b^n(t_1) \overrightarrow{l^b} \right) + \Delta\varepsilon_{ij} \tag{24}$$

The measurement model of the Extended Kalman Filter H can be derived from (24) by perturbation analysis. According to Goshen-Meskin and Bar-Itzhack (1992) and Savage (2000), the perturbation rule of the direction cosine matrix can be expressed as follows,

$$\delta C_B^{A'} = (\vec{\alpha}\times) C_B^{A'} = -\left(\vec{\theta}\times\right) C_B^{A'} \tag{25}$$

where $A'$ is an unknown coordinate frame, which is obtained by rotating a known coordinate frame $A$ with a small angle, $\vec{\alpha}$ is the rotation angle vector from $A'$ to $A$ frame, and $\vec{\theta}$ is the rotation angle vector from $A$ to $A'$ frame, and $B$ is a known coordinate frame.

Apply the perturbation rule (25) to the attitude matrix $C_b^n$, and the following relationship can be obtained,

$$\delta C_b^n = -\left(\vec{\psi}\times\right) C_b^n \tag{26}$$

where $\vec{\psi}$ is the attitude error in (17). Apply the perturbation rule (25) to both sides of the (24), the measurement model based on the time-differenced carrier phases can be obtained as,

$$\delta Y_i = -\lambda^{-1} \cdot \left[ C_e^n(t_2) \cdot \left( \overrightarrow{e_j(t_2)^e} - \overrightarrow{e_i(t_2)^e} \right) \right]^T \cdot \left( \int_{t_1}^{t_2} \overrightarrow{\delta v} \mathrm{d}t + \left( \delta C_b^n(t_2) - \delta C_b^n(t_1) \right) \overrightarrow{l^b} + \left( C_b^n(t_2) - C_b^n(t_1) \right) \overrightarrow{\delta l} \right) + \delta\Delta\varepsilon_{ij} \tag{27}$$

The first two terms in the parentheses of (27) should be expanded to establish the relationship between $\delta Y_i$ and the error state vector $x$ in (18).

According to the expression of $x$ in (19), the velocity error $\delta\vec{v}$ can be expressed as,

$$\delta\vec{v} = C_v x(t) \tag{28}$$

where $C_v$ can be derived as

$$C_v = [0 \quad I \quad 0 \quad 0 \quad 0 \quad 0 \quad 0]$$

and 0 and $I$ represent a zero matrix and an identity matrix, respectively, of three dimensions. The quantity $x(t)$ in (28) can be computed by,

$$x(t) = \phi(t, t_1)\phi(t_1, t_2)x(t_2) \tag{29}$$

where $\phi(t_i, t_j)$ is the state transfer matrix from $t_j$ to $t_i$, and its computation will be discussed later. Inserting (29) into (28), then the velocity error $\delta\vec{v}$ can be rewritten as,

$$\delta\vec{v} = C_v \phi(t, t_1)\phi(t_1, t_2)x(t_2) \tag{30}$$

According to (30), the first term in the parentheses of (27) can be expressed as follows,

$$\begin{aligned} \int_{t_1}^{t_2} \overrightarrow{\delta v} \mathrm{d}t &= \int_{t_1}^{t_2} C_v \phi(t, t_1)\phi(t_1, t_2)x(t_2)\mathrm{d}t \\ &= C_v \cdot \int_{t_1}^{t_2} \phi(t, t_1)\mathrm{d}t \cdot \phi(t_1, t_2) \cdot x(t_2) \end{aligned} \tag{31}$$

Regarding the state transfer matrix $\phi(t_i, t_j)$, the following two relationships hold (Wendel et al. 2006),

$$\phi(t + i\delta t, t + (i-1)\delta t) = I + F\delta t \tag{32}$$

$$\phi(t + (i-1)\delta t, t + i\delta t) = I - F\delta t \tag{33}$$

where $\delta t$ is the time interval of the discretization of the continuous time system (18), and $F$ is the system matrix in (18). According to (32) and (33), the following two formulae

$$\begin{aligned} \int_{t_1}^{t_2} \phi(t, t_1)\mathrm{d}t &= \sum_{i=1}^{k} \delta t \cdot \phi(t_1 + i\delta t, t_1 + (i-1)\delta t) \\ &= k\delta t(I + F\delta t) \end{aligned} \tag{34}$$

$$\phi(t_1, t_2) = \prod_{i=1}^{k} \phi(t_1 + (i-1)\delta t, t_1 + i\delta t) = (I - F\delta t)^k \tag{35}$$

can be derived, where $k$ is equal to $(t_2 - t_1)/\delta t$. By inserting (34) and (35) into (31), the first term in the parentheses of (27) can be expressed as,

$$\begin{aligned} \int_{t_1}^{t_2} \overrightarrow{\delta v} \mathrm{d}t &= \int_{t_1}^{t_2} C_v \phi(t, t_1)\phi(t_1, t_2)x(t_2)\mathrm{d}t \\ &= C_v \cdot (k\delta t(I + F\delta t)) \cdot \left( (I - F\delta t)^k \right) \cdot x(t_2) \end{aligned} \tag{36}$$

The second term in the parentheses of (27) can be expanded according to (26) as follows,

$$\begin{aligned} \left( \delta C_b^n(t_2) - \delta C_b^n(t_1) \right) \overrightarrow{l^b} = &\left( -\left(\vec{\psi}(t_2)\times\right) C_b^n(t_2) \right. \\ &\left. + \left(\vec{\psi}(t_1)\times\right) C_b^n(t_1) \right) \overrightarrow{l^b} \end{aligned} \tag{37}$$

Transform (37) and the following relationship can be obtained,

$$\begin{aligned}\left(\delta C_b^n(t_2)-\delta C_b^n(t_1)\right)\overrightarrow{l^b} &= \left(-\left(\vec{\psi}(t_2)\times\right)C_b^n(t_2)\right.\\ &\quad\left.+\left(\vec{\psi}(t_1)\times\right)C_b^n(t_1)\right)\overrightarrow{l^b}\\ &= \left(-\left(\vec{\psi}(t_2)\times\right)\left(C_b^n(t_2)-C_b^n(t_1)\right)\right.\\ &\quad\left.-\left(\left(\vec{\psi}(t_2)-\vec{\psi}(t_1)\right)\times\right)C_b^n(t_1)\right)\overrightarrow{l^b}\\ &= \left(-\left(\vec{\psi}(t_2)\times\right)\left(C_b^n(t_2)-C_b^n(t_1)\right)\right.\\ &\quad\left.-\left(\dot{\vec{\psi}}\times\right)\cdot\Delta t\cdot C_b^n(t_1)\right)\overrightarrow{l^b}\end{aligned} \tag{38}$$

where $\Delta t$ is the time interval of GPS measurement and is equal to $t_2 - t_1$. Considering the following equation (Benson 1975),

$$\dot{\vec{\psi}} = \vec{\varepsilon} - \vec{\omega}_{ic}\times\vec{\psi} \doteq \vec{\varepsilon} \tag{39}$$

The second term in the parentheses of (27) can be expressed as,

$$\begin{aligned}\left(\delta C_b^n(t_2)-\delta C_b^n(t_1)\right)\overrightarrow{l^b} &= -\left(\vec{\psi}(t_2)\times\right)\left(C_b^n(t_2)-C_b^n(t_1)\right)\overrightarrow{l^b}\\ &\quad-(\vec{\varepsilon}\times)\cdot\Delta t\cdot C_b^n(t_1)\overrightarrow{l^b}\\ &= \left(\left(\left(C_b^n(t_2)-C_b^n(t_1)\right)\overrightarrow{l^b}\right)\times\right)\vec{\psi}(t_2)\\ &\quad+\left(\left(\Delta t\cdot C_b^n(t_1)\overrightarrow{l^b}\right)\times\right)\vec{\varepsilon}\end{aligned} \tag{40}$$

By inserting (36) and (40) into (27), the measurement model based time-differenced carrier phases can be derived as follows,

$$\begin{aligned}\delta Y_i = &-\lambda^{-1}\cdot\left[C_e^n(t_2)\cdot\left(\overrightarrow{e_j(t_2)^e}-\overrightarrow{e_i(t_2)^e}\right)\right]^T\\ &\cdot\left(\left(C_v\cdot(k\delta t(I+F\delta t))\cdot\left((I-F\delta t)^k\right)\right)\cdot x(t_2)\right.\\ &+\left(\left(\left(C_b^n(t_2)-C_b^n(t_1)\right)\overrightarrow{l^b}\right)\times\right)\vec{\psi}(t_2)\\ &\left.+\left(\left(\Delta t\cdot C_b^n(t_1)\overrightarrow{l^b}\right)\times\right)\vec{\varepsilon}+\left(C_b^n(t_2)-C_b^n(t_1)\right)\overrightarrow{\delta l}\right)\\ &+\Delta\varepsilon_{ij}\end{aligned} \tag{41}$$

Define the following coefficients,

$$H_v = C_v\cdot(k\delta t(I+F\delta t))\cdot\left((I-F\delta t)^k\right) \tag{42}$$

$$H_\psi = \begin{bmatrix}0 & 0 & \left(\left(C_b^n(t_2)-C_b^n(t_1)\right)\overrightarrow{l^b}\right)\times & 0 & 0 & 0 & 0\end{bmatrix} \tag{43}$$

$$H_\varepsilon = \begin{bmatrix}0 & 0 & 0 & 0 & 0 & \left(\Delta t\cdot C_b^n(t_1)\overrightarrow{l^b}\right)\times & 0\end{bmatrix} \tag{44}$$

$$H_{\delta l} = \begin{bmatrix}0 & 0 & 0 & 0 & 0 & 0 & C_b^n(t_2)-C_b^n(t_1)\end{bmatrix} \tag{45}$$

then (41) can be rewritten as,

$$\begin{aligned}\delta Y_i = &-\lambda^{-1}\cdot\left[C_e^n(t_2)\cdot\left(\overrightarrow{e_j(t_2)^e}-\overrightarrow{e_i(t_2)^e}\right)\right]^T\\ &\cdot\left(H_v+H_\psi+H_\varepsilon+H_{\delta l}\right)\cdot x(t_2)+\Delta\varepsilon_{ij}\end{aligned} \tag{46}$$

Assuming $N+1$ satellites are observed and satellite $j$ is chosen as the reference satellite when differencing the GPS carrier phase measurements as done in (3), the total measurement model for the Extended Kalman Filter H can be expressed as,

$$y = Hx + v \tag{47}$$

where $y$, $H$, and $v$ are given by,

$$\begin{aligned}y &= \begin{bmatrix}\delta Y_1\\ \vdots\\ \delta Y_i\\ \vdots\\ \delta Y_N\end{bmatrix},\\ H &= -\lambda^{-1}\cdot\begin{bmatrix}\left[C_e^n(t_2)\cdot\left(\overrightarrow{e_j(t_2)^e}-\overrightarrow{e_1(t_2)^e}\right)\right]^T\\ \vdots\\ \left[C_e^n(t_2)\cdot\left(\overrightarrow{e_j(t_2)^e}-\overrightarrow{e_i(t_2)^e}\right)\right]^T\\ \vdots\\ \left[C_e^n(t_2)\cdot\left(\overrightarrow{e_j(t_2)^e}-\overrightarrow{e_N(t_2)^e}\right)\right]^T\end{bmatrix}\\ &\quad\cdot\left(H_v+H_\psi+H_\varepsilon+H_{\delta l}\right),\\ v &= \begin{bmatrix}\Delta\varepsilon_{1j}\\ \vdots\\ \Delta\varepsilon_{ij}\\ \vdots\\ \Delta\varepsilon_{Nj}\end{bmatrix}\end{aligned} \tag{48}$$

Please note two additional effects of the time-differencing operation. First, the satellite differencing in (3) can increase the noise level of the observables, which means that the noise vector $v$ in (48) has larger covariance than the undifferenced case. Second, cycle slips have much less side effects to the time-differenced carrier phase than to the undifferenced carrier phase. Cycle slip only affects the current measurement of the time-differenced carrier phase, while it can affect the entire subsequent carrier phase measurements. This will lead to different treatments to cycle slips in integration. For the integration of time-differenced carrier phase and INS, the time-differenced carrier phases affected by cycle slips can be simply dropped out without obvious influences to system performances. However, for the integration of carrier phase and INS, cycle slips should be restored or removed as outliers to obtain reliable navigation results.

Measurement model based on pseudoranges

The measurement model of the Extended Kalman Filter L in Fig. 3 can be derived from the observation equation of the pseudoranges, which is expressed as follows (Misra and Enge 2001),

$$\rho = r + I + T + c(\delta t_u - \delta t^s) + \xi \tag{49}$$

The ionospheric delay, $I$, can be compensated by dual-frequency measurements, the tropospheric delay, $T$, can be compensated by a model (Misra and Enge 2001), and the satellite clock error, $\delta t^s$, can be compensated by using the navigation message. Therefore, a compensated pseudorange is defined as follows,

$$\tilde{\rho} = \rho - I - T + c\delta t^s \tag{50}$$

The compensated pseudorange observation can be obtained by combining (49) and (50) as,

$$\tilde{\rho} = r + c\delta t_u + \xi \tag{51}$$

In order to remove the receiver clock error, $\delta t_u$, the compensated pseudoranges from different satellites are differenced, and a new observation

$$\tilde{\rho}^{ij} = \tilde{\rho}^i - \tilde{\rho}^j = r_i - r_j + \xi_{ij} \tag{52}$$

is obtained, where $r_i$ and $r_i$ are the geometric distance between the GPS receiver and the satellites $i$ and $j$, respectively. Supposing that the coordinates of the GPS receiver and the satellites $i$ and $j$ are $(x_{\text{gps}}, y_{\text{gps}}, z_{\text{gps}})$, $(x_i, y_i, z_i)$, and $(x_j, y_j, z_j)$, respectively, then Eq. 52 can be transformed into

$$\begin{aligned} Z_i = \tilde{\rho}^{ij} &= r_i - r_j + \xi_{ij} \\ &= \sqrt{(x_{\text{gps}} - x_i)^2 + (y_{\text{gps}} - y_i)^2 + (z_{\text{gps}} - z_i)^2} \\ &\quad - \sqrt{(x_{\text{gps}} - x_j)^2 + (y_{\text{gps}} - y_j)^2 + (z_{\text{gps}} - z_j)^2} + \xi_{ij} \end{aligned} \tag{53}$$

where $Z_i$ is a new variable introduced for convenience.

The measurement model of the Extended Kalman Filter L can be derived from (53) by perturbation analysis. By perturbing both sides of (53), the following formula can be derived,

$$\begin{aligned} \delta Z_i = &\left( \frac{x_{\text{gps}} - x_i}{r_i} - \frac{x_{\text{gps}} - x_j}{r_j}, \frac{y_{\text{gps}} - y_i}{r_i} - \frac{y_{\text{gps}} - y_j}{r_j}, \right. \\ &\left. \frac{z_{\text{gps}} - z_i}{r_i} - \frac{z_{\text{gps}} - z_j}{r_j} \right) \begin{pmatrix} \delta x_{\text{gps}} \\ \delta y_{\text{gps}} \\ \delta z_{\text{gps}} \end{pmatrix} + \delta \xi_{ij} \end{aligned} \tag{54}$$

where $(\delta x_{\text{gps}}, \delta y_{\text{gps}}, \delta z_{\text{gps}})^T$is the GPS position error vector. In order to establish the relationship between $\delta Z_i$ and the error state vector $x$ in (18), the relationship between the GPS position error and the INS position error should be studied first. Define $\vec{r}_{\text{gps}}$, $\vec{r}_{\text{ins}}$, and $\vec{l}$ to be the GPS position vector, INS position vector, and the lever arm vector between the GPS antenna and the INS center, respectively, then the following relationship holds,

$$\vec{r}_{\text{gps}} = \vec{r}_{\text{ins}} + \vec{l} \tag{55}$$

By projecting the vectors in (55) into the earth-centered earth-fixed frame (e frame), Eq. 55 can be transformed into,

$$\vec{r}^{\,e}_{\text{gps}} = C^e_n \vec{r}^{\,n}_{\text{ins}} + C^e_n C^n_b \vec{l}^{\,b} \tag{56}$$

where $C^e_n$ and $C^n_b$ are the position matrix and attitude matrix, respectively. Ignoring the position error and considering the perturbation rule of attitude matrix in (26), the perturbation to both sides of (56) produces

$$\delta \vec{r}^{\,e}_{\text{gps}} = C^e_n \left( \delta \vec{r} + C^n_b \delta \vec{l} + \left( C^n_b \vec{l}^{\,b} \right) \times \vec{\psi} \right) \tag{57}$$

where $\delta \vec{r}^{\,e}_{\text{gps}}$ is the GPS position error vector and is equal to $(\delta x_{\text{gps}}, \delta y_{\text{gps}}, \delta z_{\text{gps}})^T$. Insert (57) into (54), and the measurement model based on pseudoranges can be derived as follows,

$$\delta Z_i = G_i x + \delta \xi_{ij} \tag{58}$$

where $x$ is the error state vector presented in (18), and $G_i$ is expressed as

$$\begin{aligned} G_i = &\left[ \frac{x_{\text{gps}} - x_i}{r_i} - \frac{x_{\text{gps}} - x_j}{r_j}, \frac{y_{\text{gps}} - y_i}{r_i} - \frac{y_{\text{gps}} - y_j}{r_j}, \frac{z_{\text{gps}} - z_i}{r_i} \right. \\ &\left. - \frac{z_{\text{gps}} - z_j}{r_j} \right] \cdot C^e_n \cdot \left[ I \quad 0 \quad \left( C^n_b \vec{l}^{\,b} \right) \times \quad 0 \quad 0 \quad 0 \quad C^n_b \right] \end{aligned} \tag{59}$$

Assuming N + 1 satellites are observed and satellite $j$ is chosen as the reference satellite when differencing the GPS pseudoranges, the total measurement model for the Extended Kalman Filter L can be expressed as,

$$z = Gx + w \tag{60}$$

where $z$, $G$, and $w$ are

$$z = \begin{bmatrix} \delta Z_1 \\ \vdots \\ \delta Z_i \\ \vdots \\ \delta Z_N \end{bmatrix}, \quad G = \begin{bmatrix} G_1 \\ \vdots \\ G_i \\ \vdots \\ G_N \end{bmatrix}, \quad w = \begin{bmatrix} \Delta \xi_{1j} \\ \vdots \\ \Delta \xi_{ij} \\ \vdots \\ \Delta \xi_{Nj} \end{bmatrix} \tag{61}$$

Equations 60 and 61 formulate the measurement model based on pseudoranges.

**Table 1** Noise parameters of inertial sensors used

| Noise parameters | Noise values |
|---|---|
| Gyro channel | |
| Bias (deg/h) | 30 |
| Bias in run stability from turn-on (deg/h) | 5 |
| Scale factor stability (ppm) | 500 |
| Angle random walk (deg/root-h) | 0.09 (max.), 0.035 (norm.) |
| Rate noise (deg/h) | 360 (max.) |
| Accelerometer channel | |
| Bias (milli-g) | 4 |
| Bias in run stability from turn-on (micro-g) | 500 |
| Scale factor stability (ppm) | 800 |
| Velocity random walk (micro-g/root-Hz) | 180 (max.), 60 (norm.) |
| Acceleration noise (milli-g) | 400 (max.), 100 (norm.) |

## Experimental tests and analysis

Field tests were carried out to evaluate the performances of the proposed dual-rate Kalman Filter-based GPS/INS integrated navigation system. A tactical grade INS was used, which includes three quartz rate sensors (QRS) and three vibrating quartz accelerometers (VQA). The performance parameters of the inertial sensors are listed in Table 1. For GPS, a Leica Gx1230 receiver was used with a Leica Leiat502 antenna. GPS PPK (Post-Processing Kinematic) positioning solutions were used to provide the position reference for the GPS/INS integrated system. In our tests, the GPS base station was located on the top of Electrical Engineering, UNSW, with a Leica Mc500 receiver and a Leica Leiat504 Leis antenna.

Below, the performances of the proposed dual-rate Kalman Filter (DRKF)-based GPS/INS integration will be compared with those of the conventional integration, namely the tightly coupled integration of GPS/INS discussed in "Review of GPS/INS integration for navigation applications", regarding two aspects: the coasting performance and the navigation accuracy.

### Coasting performance comparison and analysis

For land vehicle navigation, GPS signals can be easily blocked by trees, bridges, or city canyons. The coasting performance of the GPS/INS integrated system is the performance of the system when the GPS signals are unusable. For a tactical INS, the inertial sensors suffer from large drifts, which constrains the free operation time of the INS, so the coasting ability is an important criteria for the integration of GPS and tactical INS. For a given GPS/INS integrated system, the coasting performance is mainly determined by whether the drifts of the inertial sensors are well compensated. If the drifts of the inertial sensors are well estimated and compensated when the GPS signals are intact, the system will have a better coasting performance during the subsequent GPS signals outages.

A field test was carried out to evaluate the coasting performances of the integrated navigation systems. The arrangement of the IMU and the GPS antenna, and the size of the lever arm between the IMU center and the GPS antenna phase center are shown in Fig. 4. The test trajectory is shown in Fig. 5.

The observed satellites with elevation angles above 15° during the test are shown in Fig. 6. It can be noted that the number of satellites was not less than five at any time during the test period, which means that GPS signal blockage did not occur. In order to evaluate the coasting performance of the integrated navigation system, several GPS signal blockages were simulated. The experimental procedure is as follows:

1. According to the rover and base GPS data, compute the reference navigation solutions by using the PPK positioning algorithm.

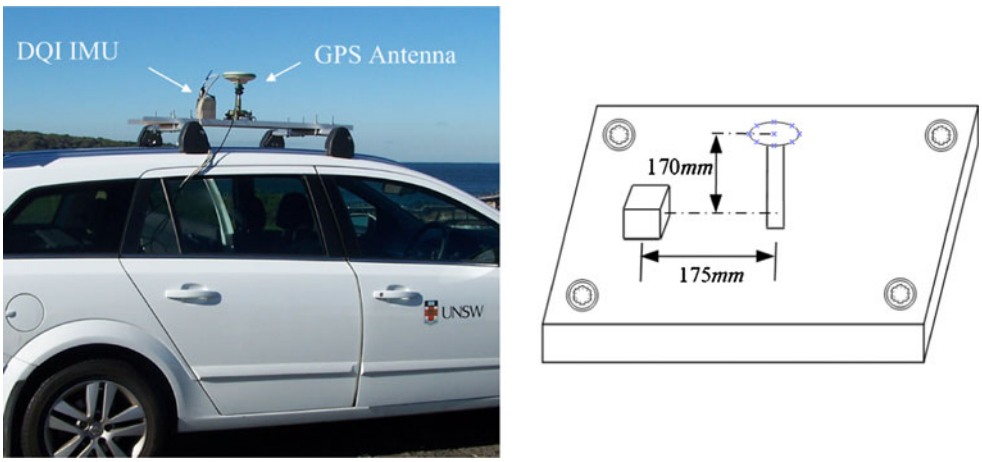


**Fig. 4** The arrangement of IMU and GPS antenna, and the size of the lever arm between the IMU center and the GPS antenna phase center

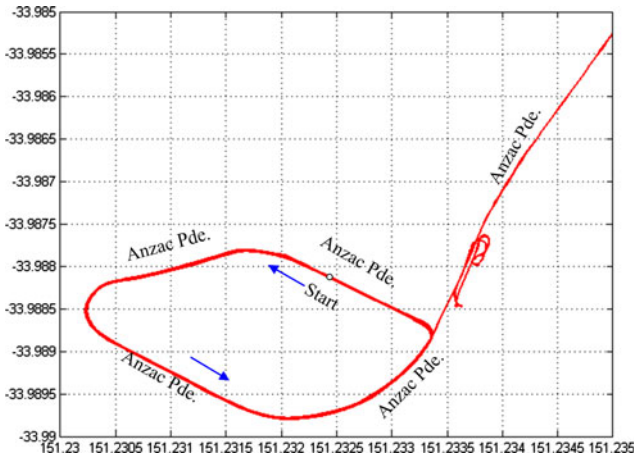


**Fig. 5** The test trajectory for the coasting performance evaluation

2. Randomly select several time intervals in the experimental process as the simulated coasting intervals.
3. Carry out normal integrated navigation computation and calibrate the inertial sensors outside the simulated coasting intervals.
4. Carry out pure inertial navigation computation inside the simulated coasting intervals and obtain the coasting navigation solutions.
5. Compare the coasting navigation solutions and the reference navigation solutions to compute the navigation errors during the coasting intervals.

The selection of the simulated coasting intervals should be carefully done. If the time interval is too long, the coasting performance evaluation will be meaningless, because the tactical INS cannot last very long by itself. So five 60-s time intervals, as shown in Table 2, were selected in our experiment.

The coasting errors of the DRKF-based integration and the conventional integration are shown in Figs. 7 and 8, respectively. The coasting errors comparison between the DRKF-based integration and the conventional integration for different time intervals are listed in Table 3.

**Table 2** Simulated coasting intervals

| Coasting no. | Coasting time span GPS time (s) | Coasting time interval (s) |
|---|---|---|
| 1 | 440,001–440,060 | 60 |
| 2 | 440,501–440,560 | 60 |
| 3 | 441,001–441,060 | 60 |
| 4 | 441,501–441,560 | 60 |
| 5 | 442,001–442,060 | 60 |

From Table 3, and Figs. 7 and 8, it can be noted that:

1. For the coasting intervals less than 30 s, the coasting errors of the DRKF-based integration are reduced to less than 10 m, reaching the accuracy of GPS SPS (standard positioning service), and the coasting ability of this integration improves about two times compared to that of the conventional integration.
2. For the coasting interval of 60 s, the coasting ability of the DRKF-based integration is similar to that of the conventional integration.

## Navigation accuracy comparison and analysis

A field test was carried out to evaluate the accuracy of the integrated navigation systems. The arrangement of the IMU and the GPS antenna, and the size of the lever arm between the IMU center and the GPS antenna phase center are shown in Fig. 9. The test trajectory is shown in Fig. 10.

The observed satellites with elevation angles above 15° during the test are shown in Fig. 11. It can be noted from this figure that the GPS observation environment was very poor during the test, and many GPS signal blockages occurred. Because the coasting performances of the integrated systems have been evaluated in the previous

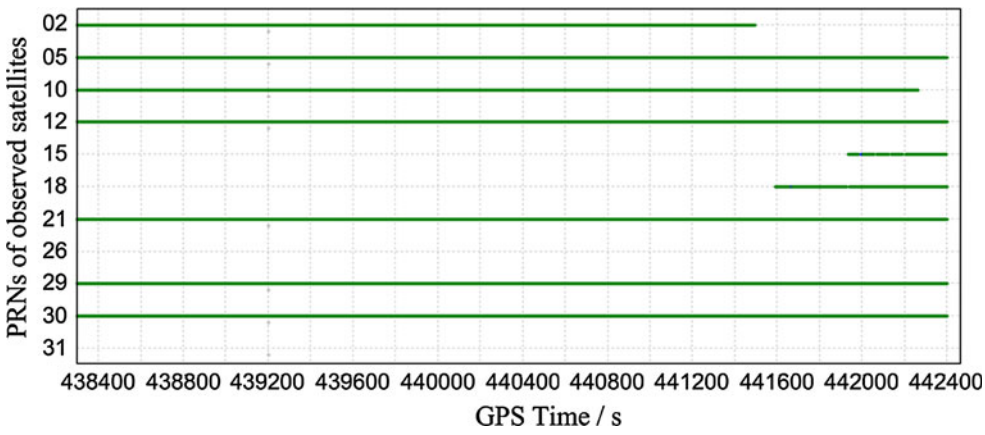


**Fig. 6** The observed satellites with elevation angles above 15° during the test

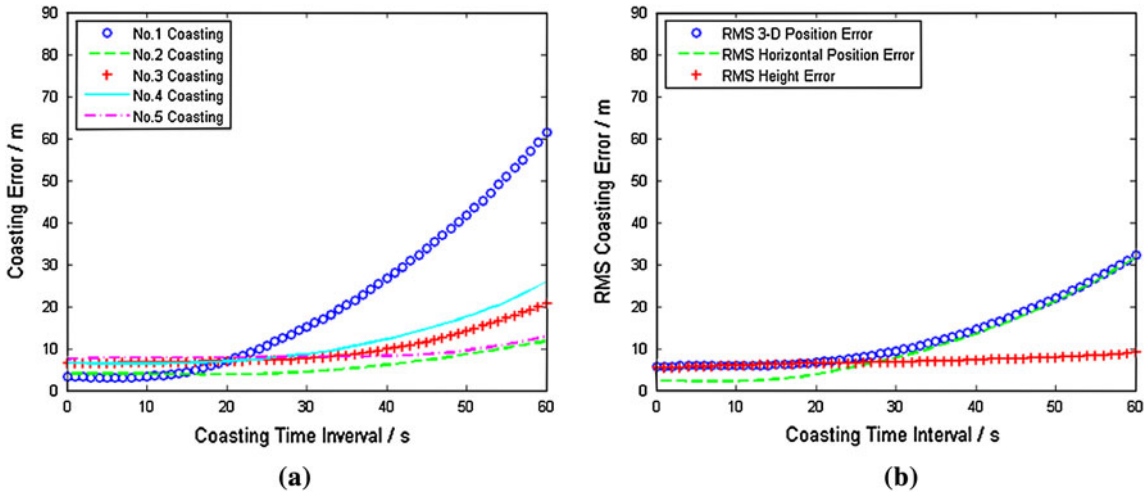


**Fig. 7** Coasting error and RMS coasting error of the DRKF-based integration. **a** coasting error, **b** RMS coasting error

**Table 3** Coasting errors comparison between the DRKF-based integration and the conventional integration

| Time interval (s) | DRKF-based integration | | | Conventional integration | | |
|---|---|---|---|---|---|---|
| | 3-D position error (m) | Horizontal position error (m) | Height error (m) | 3-D position error (m) | Horizontal position error (m) | Height error (m) |
| 5 | 5.83 | 2.22 | 5.63 | 7.08 | 5.55 | 4.39 |
| 10 | 5.90 | 2.24 | 5.94 | 9.34 | 8.09 | 4.69 |
| 20 | 6.67 | 3.85 | 6.42 | 17.43 | 16.58 | 5.37 |
| 30 | 9.43 | 7.81 | 6.72 | 27.86 | 27.15 | 6.28 |
| 40 | 14.53 | 13.52 | 7.23 | 39.68 | 38.96 | 7.53 |
| 50 | 21.99 | 21.31 | 7.85 | 52.71 | 51.95 | 8.89 |
| 60 | 32.15 | 31.62 | 8.95 | 67.75 | 66.92 | 10.62 |

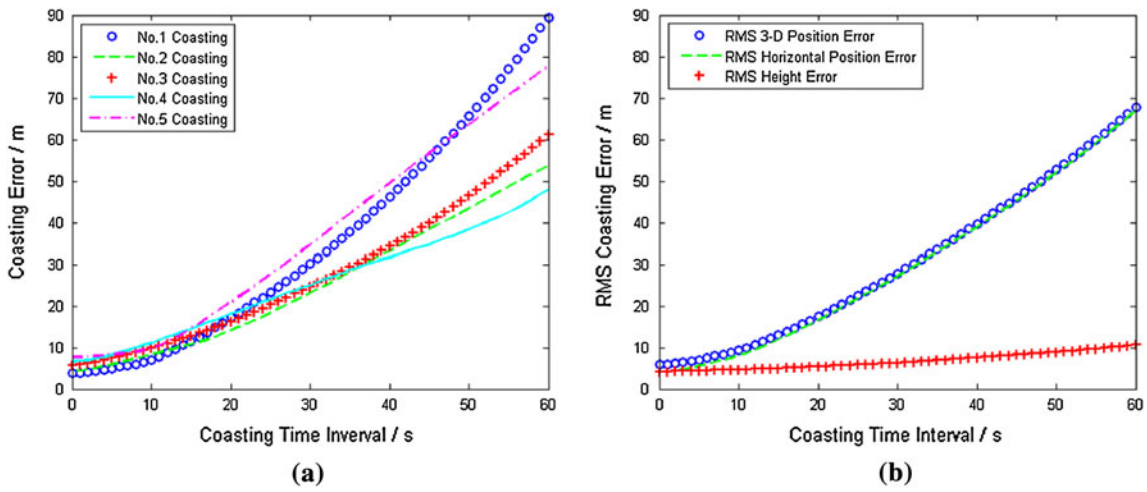


**Fig. 8** Coasting error and RMS coasting error of the conventional integration. **a** coasting error, **b** RMS coasting error

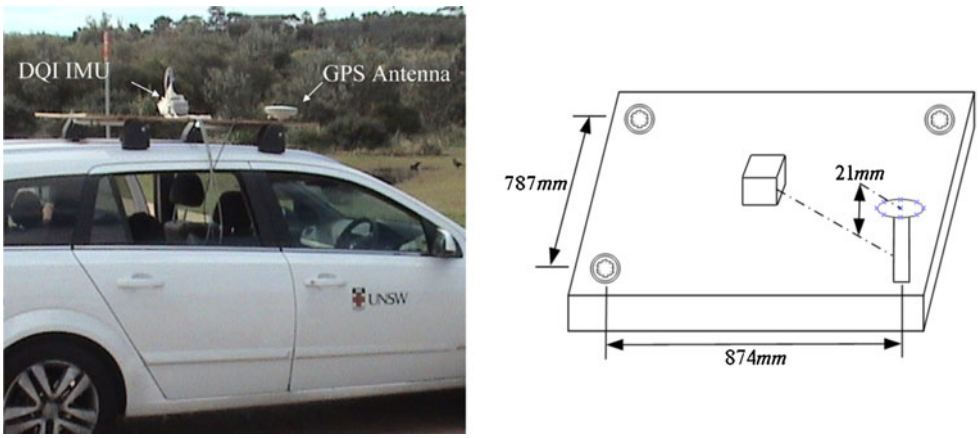


**Fig. 9** The arrangement of IMU and GPS antenna, and the size of the lever arm between the IMU center and the GPS antenna phase center

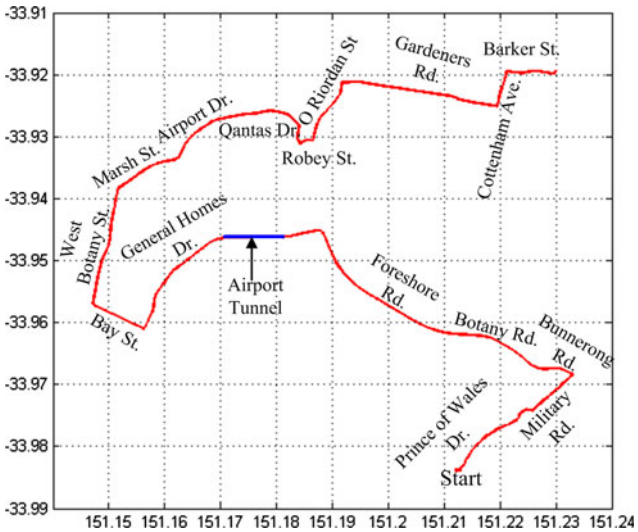


**Fig. 10** The test trajectory for the navigation accuracy evaluation

**Table 4** The navigation accuracy comparison

| | DRKF-based integration | Conventional integration |
|---|---|---|
| $(\Delta r_N)_{\mathrm{RMS}}$ (m) | 0.82 | 1.17 |
| $(\Delta r_E)_{\mathrm{RMS}}$ (m) | 0.77 | 1.15 |
| $(\Delta h)_{\mathrm{RMS}}$ (m) | 2.46 | 4.00 |
| $(\Delta r)_{\mathrm{RMS}}$ (m) | 2.70 | 4.32 |
| $(\Delta r)_{\mathrm{Max}}$ (m) | 10.31 | 19.74 |
| $(\Delta v_N)_{\mathrm{RMS}}$ (m/s) | 0.39 | 0.69 |
| $(\Delta v_E)_{\mathrm{RMS}}$ (m/s) | 0.31 | 0.69 |
| $(\Delta v_D)_{\mathrm{RMS}}$ (m/s) | 0.14 | 0.40 |
| $(\Delta v)_{\mathrm{RMS}}$ (m/s) | 0.45 | 1.06 |
| $(\Delta v)_{\mathrm{Max}}$ (m/s) | 2.31 | 6.63 |
| $(\psi_N)_{\mathrm{RMS}}(')$ | 0.67 | 2.68 |
| $(\psi_E)_{\mathrm{RMS}}(')$ | 0.56 | 2.56 |
| $(\psi_D)_{\mathrm{RMS}}(')$ | 2.93 | 10.56 |

**Fig. 11** The observed satellites with elevation angles above 15° during the test

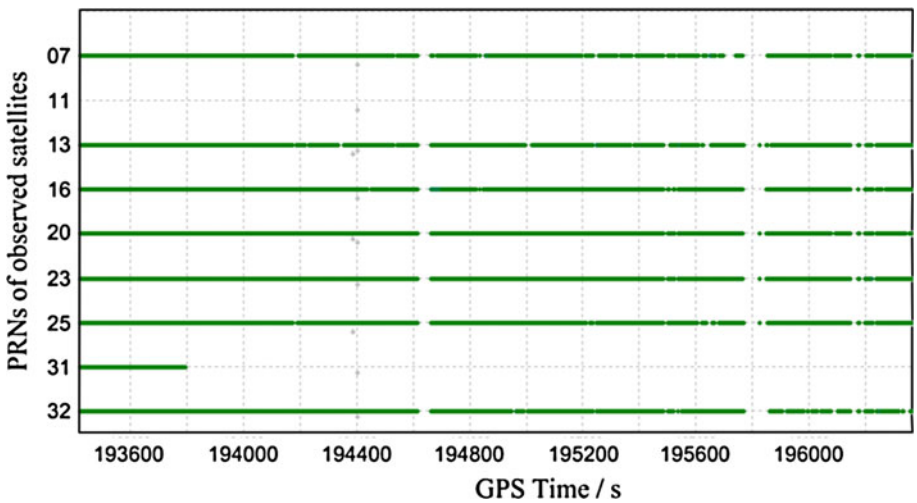

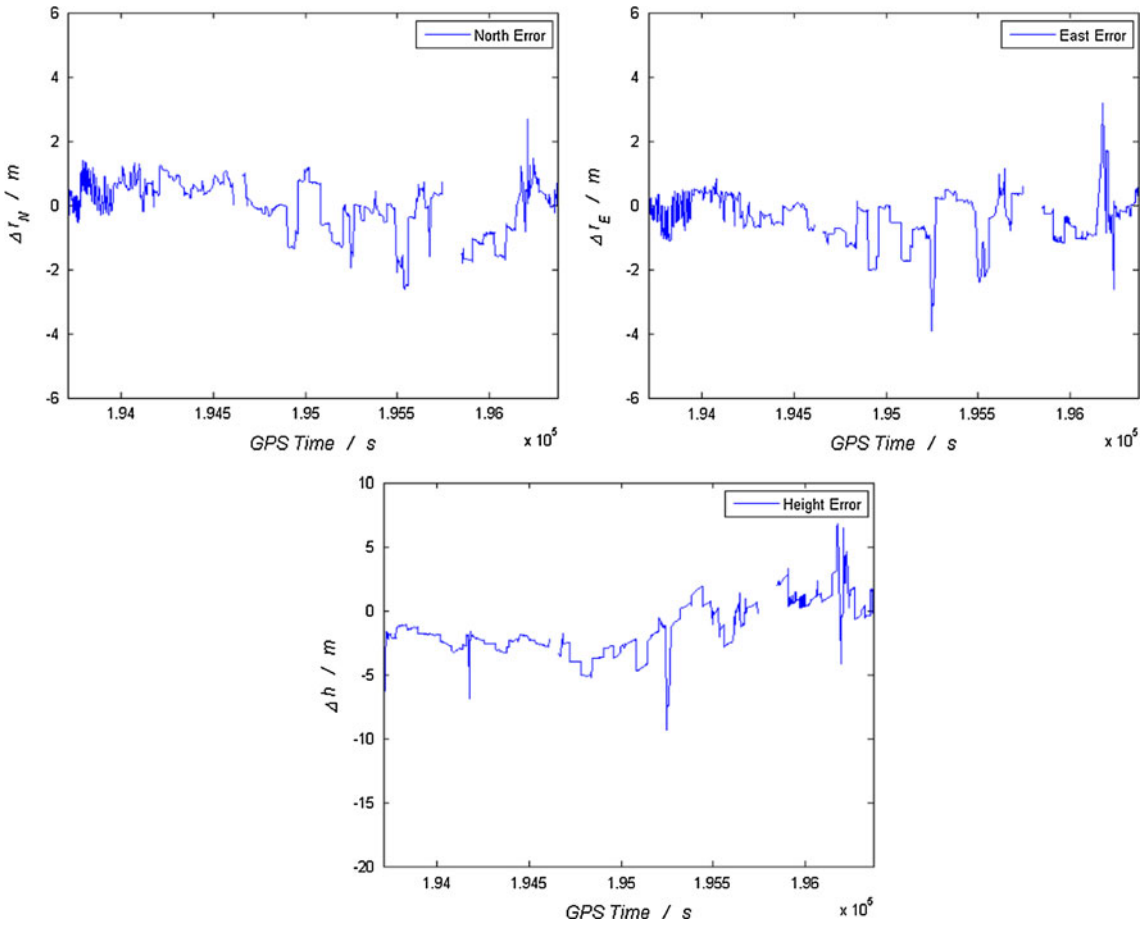


**Fig. 12** The position errors of the DRKF-based integration

subsection, this subsection will only evaluate navigation accuracy by using the GPS PPK positioning solutions as the navigation reference.

The position errors of the DRKF-based integration and the conventional integration are shown in Figs. 12 and 13. The comparison of navigation errors comparison between the DRKF-based integration and the conventional integration are listed in Table 4.

From Table 4, and Figs. 12 and 13, it can be noted that the position, velocity, and attitude accuracy of the DRKF-based integration are much better than those of the conventional integration.

## Conclusions and future work

We discussed a new design for GPS/INS integrated navigation system. In contrast to other existing GPS/INS integration schemes, this design has implemented the GPS/INS integration for the first time by using a dual-rate Kalman Filter. The GPS pseudoranges and the time-differenced GPS carrier phases are integrated with INS measurements through the dual-rate Kalman Filter. The experimental test results have shown that, compared with the conventional GPS/INS integrated navigation system, the proposed dual-rate Kalman Filter–based GPS/INS integration dramatically improves the coasting performance and the navigation accuracy.

It can be noted that, although the time-differenced GPS carrier phase has millimeter-level accuracy, the navigation accuracy of the DRKF-based GPS/INS integration is still at the meter level, as shown in Table 4. This is because the errors of the GPS pseudoranges are introduced into the system through the low-rate Kalman Filter, as shown in Fig. 3. In order to further improve the navigation accuracy, the original carrier phases can be used in the low-rate Kalman Filter instead of the pseudoranges. The integer ambiguities of the carrier phases can be resolved in parallel to the processing of the high-rate Kalman Filter, and when the integer ambiguities are fixed correctly, the unambiguous carrier phases can be input into the low-rate Kalman Filter. In the framework of the proposed DRKF-based

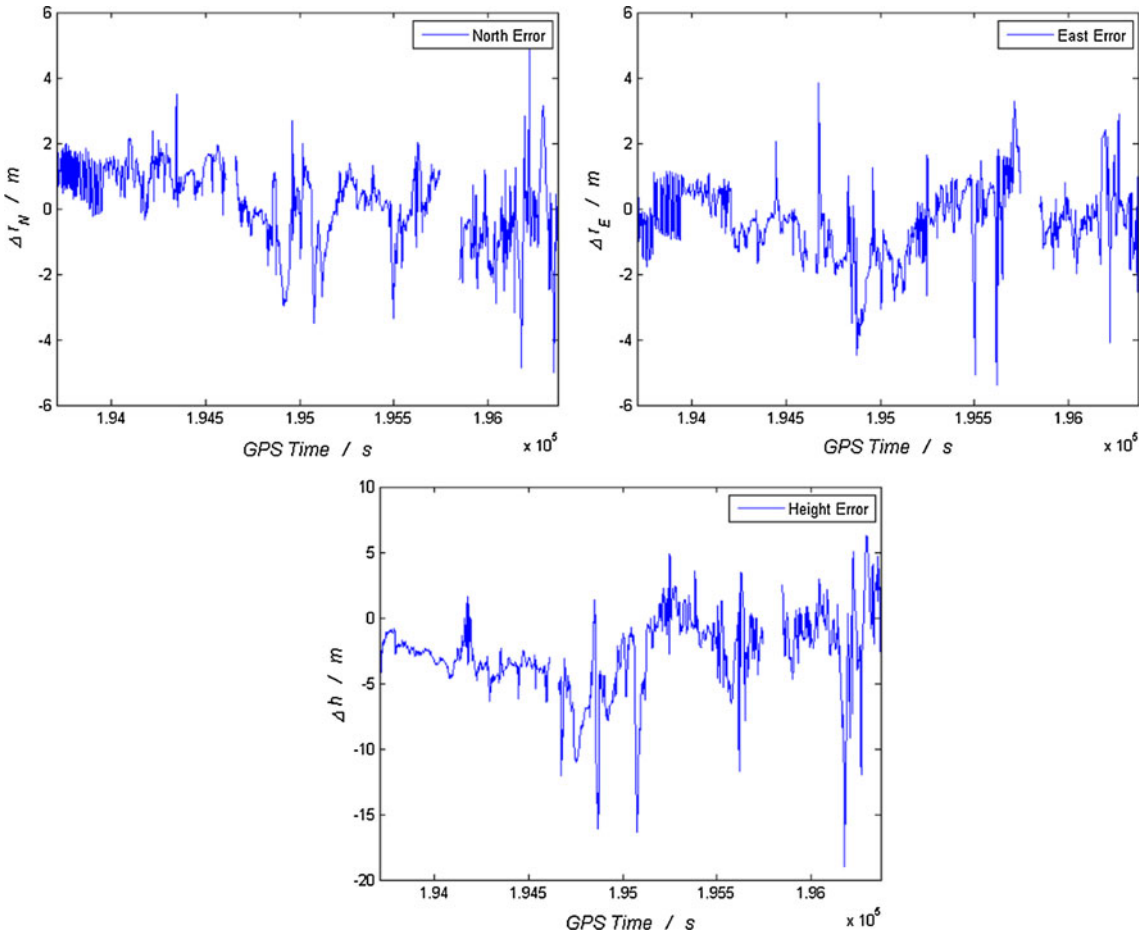


**Fig. 13** The position errors of the conventional integration

integration, this is a potential to further improve the navigation accuracy with the future generation of Global Navigation Satellite Systems.

**Acknowledgments** The first author would like to show his appreciation to Chinese Scholarship Council for supporting his PhD study at the University of New South Wales (UNSW) in Australia. The authors also would like to thank Dr. Weidong Ding, Mr. Ali Almagbile, and Mr. Nathan Knight in the School of Surveying and Spatial Information Systems at UNSW, for their help during the experimental tests.

## References

Banville S, Langley RB (2009) Improving real-time kinematic PPP with instantaneous cycle-slip correction. ION GNSS 2009, Savannah, Georgia, USA, pp 2470–2478

Benson DO (1975) Comparison of two approaches to pure-inertial and Doppler-inertial error analysis. IEEE Trans Aerosp Electron Syst 11(4):447–455

Farrell JL (2001) Carrier phase processing without integers. ION 57th Annual Meeting, Albuquerque, NM, USA

Farrell JL (2006) Velocity and acceleration from unaided carrier phase. IEEE/ION PLANS 2006, Coronado, CA, USA

Gebre-Egziabher D, Wang J (1998) Gravity modeling for high-accuracy GPS/INS integration. Navigation 45(3):209–220

Goshen-Meskin D, Bar-Itzhack IY (1992) Unified approach to inertial navigation system error modeling. J Guid Control Dyn 15(3):648–653

GPS SPS PS (2008) Global positioning system standard positioning service performance standard, 4th edn. DoD Official Document, Washington, pp 21–22

Graas FV, Soloviev A (2004) Precise velocity estimation using a stand-alone GPS receiver. Navigation 51(4):283–292

Grewal MS, Weill LR, Andrews AP (2007) Global positioning systems, inertial navigation, and integration, 2nd edn. Wiley, New York, pp 382–424

Groves PD (2008) Principles of GNSS, inertial, and multisensor integrated navigation systems, 3rd edn. Artech House, London, pp 363–406

Han S, Wang J (2008) Monitoring the degree of observability in integrated GPS/INS systems. In: International symposium on GPS/GNSS 2008, Tokyo, Japan, pp 414–421

Han S, Wang J (2010) Land vehicle navigation with the integration of GPS and reduced INS: performance improvement with velocity aiding. J Navig 63(1):153–166

IS-GPS-200D (2006) Navistar global positioning system interface specification. Navstar GPS Joint Program Office, El Segundo, p 84

Jekeli C (1997) The effect of earth's gravity on precise short-term, 3-D free-inertial navigation. Navigation 44(3):347–357

Misra P, Enge PK (2001) The global positioning system: signals, measurements, and performance. Ganga-Jamuna Press, Lincoln, pp 153–155, 161–170, 175–250

Niu X, El-Sheimy N (2005) The development of a low-cost MEMS IMU/GPS navigation system for land vehicles using auxiliary velocity updates in the body frame. ION GNSS 2005, Long Beach, CA, USA, pp 13–16

Savage PG (1998) Strapdown inertial navigation integration algorithm design part 1: attitude algorithms. J Guid Control Dyn 21(1):19–28

Savage P (2000) Strapdown analytics. Strapdown Associates, MN, pp 3-76–3-86

Wang J, Stewart MP, Tsakiri M (1998) A discrimination test procedure for ambiguity resolution on the fly. J Geodesy 72(11):644–653

Wang J, Stewart MP, Tsakiri M (2000) A comparative study of the integer ambiguity validation procedures. Earth Planets Space 52(10):813–817

Wang J, Lee HK, Hewitson S et al (2003) Influence of dynamics and trajectory on integrated GPS/INS navigation performance. J Glob Position Syst 2(2):109–116

Wendel J, Trommer GF (2004) Tightly coupled GPS/INS integration for missile applications. Aerosp Sci Technol 8(7):627–634

Wendel J, Monikes R, Trommer GF (2006) Time-differenced carrier phase measurements for tightly coupled GPS/INS integration. IEEE/ION PLANS 2006, Coronado, CA, USA

Zheng G, Gebre-Egziabher D (2009) Enhancing ambiguity resolution performance using attitude determination constraints. ION GNSS 2009, Savannah, GA, USA, pp 2156–2168

## Author Biographies

**Songlai Han** He received a B.Sc. degree in Electronic Science and Technology from Tianjin University, Tianjin, P. R. China, in 2003; a M.Sc. degree in Control Science and Technology from National University of Defense Technology, Changsha, P. R. China, in 2005; and a Ph.D. degree in Optic Engineering from National University of Defense Technology, Changsha, P. R. China, in 2010. He is currently a lecturer in the College of Optoelectric Science and Engineering, National University of Defense Technology, P. R. China. His current research interests include INS, GPS/INS integration, multi-sensor fusion, and stochastic theory and its applications in navigation systems.

**Jinling Wang** He received a B.Sc. degree in Surveying/GNSS from Wuhan Technical University of Surveying & Mapping, Wuhan, P. R. China, in 1983; a M.Sc. degree in Surveying/GNSS from Wuhan Technical University of Surveying & Mapping, Wuhan, P. R. China, in 1990; and a Ph.D. degree in GPS/Geodesy from Curtin University, Perth, Australia in 1999. He is currently an Associate Professor in the School of Surveying & Spatial Information Systems, University of New South Wales, Sydney, Australia. His current research interests include Global Navigation Satellite Systems and their integration, augmentation of GPS with pseudolites, integration of INS and GPS/GLONASS, and statistical theory and its applications in positioning and navigation systems: http://www.gmat.unsw.edu.au/wang.